

Lesch-Nyhan disease causes impaired energy metabolism and reduced developmental potential in midbrain dopaminergic cells

Scott Bell,^{1,2,10} Vincent McCarty,^{1,2,10} Huashan Peng,^{1,2} Malvin Jefri,^{1,2} Nuwan Hettige,^{1,2} Lilit Antonyan,^{1,2} Liam Crapper,^{1,2} Liam A. O'Leary,^{1,2} Xin Zhang,^{1,2} Ying Zhang,^{1,2} Hanrong Wu,^{1,2} Diane Sutcliffe,^{3,4,5} Iliaria Kolobova,^{1,2} Thad A. Rosenberger,⁶ Luc Moquin,² Alain Gratton,² Jelena Popic,^{7,8} Ilse Gantois,^{7,8} Patrick S. Stumpf,⁹ Andreas A. Schuppert,⁹ Naguib Mechawar,² Nahum Sonenberg,^{7,8} Michel L. Tremblay,^{7,8} Hyder A. Jinnah,^{3,4,5} and Carl Ernst^{1,2,*}

¹Psychiatric Genetics Group, McGill University, Montreal, QC, Canada

²Department of Psychiatry, McGill University and Douglas Hospital Research Institute, 6875 LaSalle Boulevard, Frank Common Building, Room 2101.2, Montreal, QC H4H 1R3, Canada

³Department of Neurology, Emory University, Atlanta, GA, USA

⁴Department of Human Genetics, Emory University, Atlanta, GA, USA

⁵Department of Pediatrics, Emory University, Atlanta, GA, USA

⁶Department of Pharmacology, Physiology, and Therapeutics, School of Medicine and Health Sciences, University of North Dakota, Grand Forks, ND, USA

⁷Department of Biochemistry, McGill University, Montreal, QC, Canada

⁸Rosalind and Morris Goodman Cancer Research Centre, McGill University, Montreal, QC, Canada

⁹Joint Research Center for Computational Biomedicine, RWTH Aachen University, Aachen, Germany

¹⁰These authors contributed equally

*Correspondence: carl.ernst@mcgill.ca

<https://doi.org/10.1016/j.stemcr.2021.06.003>

SUMMARY

Mutations in *HPRT1*, a gene encoding a rate-limiting enzyme for purine salvage, cause Lesch-Nyhan disease which is characterized by self-injury and motor impairments. We leveraged stem cell and genetic engineering technologies to model the disease in isogenic and patient-derived forebrain and midbrain cell types. Dopaminergic progenitor cells deficient in *HPRT* showed decreased intensity of all developmental cell-fate markers measured. Metabolic analyses revealed significant loss of all purine derivatives, except hypoxanthine, and impaired glycolysis and oxidative phosphorylation. real-time glucose tracing demonstrated increased shunting to the pentose phosphate pathway for *de novo* purine synthesis at the expense of ATP production. Purine depletion in dopaminergic progenitor cells resulted in loss of RHEB, impairing mTORC1 activation. These data demonstrate dopaminergic-specific effects of purine salvage deficiency and unexpectedly reveal that dopaminergic progenitor cells are programmed to a high-energy state prior to higher energy demands of terminally differentiated cells.

INTRODUCTION

Lesch-Nyhan disease (LND) is a rare genetic condition characterized by severe motor impairment, dystonia, crystals in the urine, and self-mutilation (Jinnah et al., 2006; Lesch and Nyhan, 1964). It is caused by sequence errors in *HPRT1*, which encodes the protein hypoxanthine-guanine phosphoribosyl transferase (HPRT), a critical enzyme in purine recycling. HPRT adds a phospho-ribose group to breakdown products of purine metabolism, guanine or hypoxanthine, and converts these to guanosine monophosphate (GMP) or inosine monophosphate (IMP), respectively. Deficiency of HPRT presents as a “spectrum disorder,” with only those with enzymatic activity under ~2% showing behavioral and neurological impairment, including self-injury and motor anomalies. Those with enzymatic activity greater than 2% are called LN variants (LNVs) or “attenuated variants” (Jinnah et al., 2010). These cases are subcategorized into those with hyperuricemia (greater than ~8% enzymatic activity) or those with hyperuricemia and neurological dysfunction but no self-injury

(>1% enzymatic activity) (Jinnah et al., 2010). Since *HPRT1* is located on the X chromosome, both LND and LNV follow an X-linked recessive pattern of inheritance and thus present almost exclusively in boys.

Previous research into LND has used a variety of models, both *in vivo* and *in vitro* (Bell et al., 2016). *In vitro* studies used accessible somatic cells from outside the central nervous system, such as fibroblasts (Costa et al., 1980; Cox et al., 1970; Edelstein et al., 1978; Jinnah, 2009), which were informative on the nature of genetic variants leading to LND but provided limited information about the neurological changes that underpinned its most dramatic symptoms (Costa et al., 1980). A more clinically relevant model of Lesch-Nyhan spectrum disorders would ideally be made in neuronal cells, a technique now available (Takahashi et al., 2007), which may help to answer long-standing questions in LND research.

Beyond the genetic mutations in *HPRT1*, the pathogenesis of LND remains unknown, although there exist clinical, human neuroanatomical, and mouse knockout (KO) studies suggesting midbrain dopaminergic cell involvement.





Positron emission tomography imaging and postmortem brain studies have indicated that the brains of LND patients are broadly normal, but show significantly reduced dopamine and tyrosine hydroxylase (TH) levels (Ernst et al., 1996; Göttle et al., 2014; Watts et al., 1982). Postmortem data suggest that cell markers of midbrain dopaminergic cell identity are present in midbrain basal ganglia cells but at decreased intensity levels, without a morphological correlate; that is, cell number, density, and appearance look grossly normal (Göttle et al., 2014). This observation and others led to a “developmental” hypothesis of LND (Egami et al., 2007; Lewers et al., 2008), whereby purine salvage may be required at some stage during midbrain dopaminergic cell development for these cells to terminally differentiate.

Cell models used to investigate the neurobiology of LND have been HPRT-deficient cancerous cell lines obtained from human brain tumors. These lines were able to recapture many aspects of human neural biology and predicted HPRT dysfunction, such as a reduction in dopamine (DA) production (Bitler and Howard, 1986) and dopaminergic differentiation (Yeh et al., 1998); however, immortalized cell lines were also found to possess qualities that confounded the results because of their variable genomes (Paul et al., 2007) and unstable differentiation into the dopaminergic lineage (Gao et al., 2016). Rodent *Hprt1* KO studies have shown little to no behavioral phenotype, but significant decreases in DA levels in the midbrain (Jin-nah, 2009).

Cells produce purines by synthesizing them *de novo* or by recycling breakdown products, the latter of which is dependent on HPRT. In *de novo* purine synthesis, and beginning from cellular glucose uptake, glucose derivatives are shunted via the pentose phosphate pathway (PPP) (Pedley and Benkovic, 2017) to become 5-carbon pentose sugars such as ribose-5-phosphate (R5P) (Pedley and Benkovic, 2017), which can then be used for other cellular needs, including purine synthesis. The first committed steps from a pentose sugar into the series of reactions that make up purine synthesis is that from R5P to phosphoribosyl diphosphate (PRPP). PRPP enters a series of enzymatic reactions requiring inputs such as glutamine, ATP, and folate derivatives (Moffatt and Ashihara, 2002), and generates several intermediate products such as 5-aminoimidazole-4-carboxamide ribonucleotide (AICAR). The final product of the *de novo* purine synthesis pathway, IMP, is readily converted to GMP or AMP. These ribonucleotide products are widely used in the cell for a variety of purposes, including DNA/RNA synthesis and energy storage via production of ATP and GTP. Eventually, adenine and guanine may be degraded into hypoxanthine and xanthine. If no HPRT-dependent recycling occurs, these waste metabolites are secreted as uric acid (Moffatt and Ashihara, 2002).

Cells have different energy sensors to cope with changing energy states. One important sensor is AMP-activated protein kinase (AMPK), which senses the ratio of AMP to ATP; an increased ratio activates the enzyme to drive other metabolic pathways to increase ATP (Garcia and Shaw, 2017). The mTORC (mammalian target of rapamycin complex) axis is a signaling pathway that can integrate growth factor/second messenger signals (e.g., FGF/EGF-PI3-AKT) and cell nutrient status (e.g., purines and amino acids) to affect cell growth, ribosome synthesis, autophagy, ciliary dynamics, and protein translation (Emmanuel et al., 2017; Saxton and Sabatini, 2017). One key brake on mTORC1 is the TSC1/2 complex, which inhibits the activation of the mTORC1 activator RHEB (Hoxhaj et al., 2017). RHEB is a purine sensor; a loss of purines depletes RHEB, reducing mTORC1 activation (Emmanuel et al., 2017).

mTORC1 is associated with cell differentiation and promotes cell maturation. Engineered mutations in the *Mtor* gene cause embryonic lethality in mice (Murakami et al., 2004), and selective deletion in brain causes major brain alterations (Garza-Lombó and Gonsebatt, 2016; Ka et al., 2014), including deficits in progenitor cell self-renewal. Across other cell types, induced mutations impairing mTORC1 lead to loss of differentiation potential (La et al., 2018; Wang et al., 2016), suggesting that activation of mTORC1 may be important in allowing cells to develop to their full potential.

Here we address long-standing questions about HPRT deficiency in the human nervous system. We find that loss of HPRT has remarkably selective effects in midbrain dopaminergic cells, specifically in reduced ATP production and decreased mTORC1 activation. These effects may drive developmental loss of expression in critical genes such as FOXA1/2 needed for dopaminergic cell terminal differentiation.

RESULTS

Simultaneous generation of midbrain dopaminergic and forebrain cortical progenitor cells reveals dopaminergic cell-specific effects of purine salvage deficiency on expression of essential developmental markers

We made two different clonal *HPRT1* KO lines, both isogenic with a single healthy donor line (Figures S1A and S1B), using our simultaneous reprogramming/gene editing technique (Bell et al., 2019). We used two separate induced pluripotent stem cell (iPSC) clones from this donor cell and refer to these clones as control 1 and control 2. Upon reaching a pluripotent state, iPSCs were assessed for markers of pluripotency in both KO and control states, and we observed no differences in



ability to make iPSCs or marker intensity across cell lines (Figures S1C and S1D). Loss of HPRT thus has no effect on stem cell induction or maintenance of iPSCs, despite clear expression of HPRT in this cell type. All iPSCs were assessed for genomic integrity using a next-generation sequencing assay of 5,209 genes, found approximately equally across chromosomes. The resolution of detection for chromosomal anomalies was ≥ 10 Mb. Next, we simultaneously differentiated each iPSC line independently to distinct populations of midbrain DAergic (DA) and forebrain cortical (CN) neural progenitor cells (NPCs), using gold standard assays that we have previously published for each cell type (Bell et al., 2019; Jeffri et al., 2020). Simultaneous differentiation allows us to control for operator, time-of-day, and media batch effects of common reagents used to derive CN or DA NPCs from iPSCs. Quality control parameters include staining both NPC types and 30-day-differentiated cells with markers for both CN and DA cells relevant to each time point (Figure S2). The DA marker FOXA2 stained exclusively DA NPCs, while TH was found only in differentiated DA neurons (Figures S2A and S2B). FOXC1 was absent from midbrain cells but present in both CN NPCs and CN neurons (Figures S2C and S2B). Electrophysiological properties of DA neurons showed characteristic features of midbrain DA cells, including high-frequency bursting activity (Figure S2E) and a depolarizing sag in response to current clamp hyperpolarization followed by action potential trains (Figure S2F). Direct immunocytochemical comparison of both CN and DA NPCs made simultaneously for both *HPRT1* KO and isogenic controls revealed unambiguous decreases in intensity of all DA markers in *HPRT1* KOs, although all markers were detected in almost all cells (Figures 1A–E). Quantification by western blot and using an expanded range of markers further supported this finding (Figure 1F; FOXA1, 73% \pm 11% [$p = 0.0098$] decrease; FOXA2, 76% \pm 8.6% [$p = 0.0074$] decrease; LMX1A, 34% \pm 10% [$p = 0.0408$] decrease). Assessment of cell death showed slight but significantly less cell death (Figures S3A and S3B) in KO cells. We found no discernible difference for *HPRT1* KO in CN NPCs for any markers, suggesting that loss of HPRT may lead to relatively specific effects in DA NPCs. Such drastic decreases in the intensity of DA markers in this committed progenitor cell type suggests that loss of HPRT affects early stages of developmental programming in DA cells but not CN cells. The detection of DA markers with less intensity in *HPRT1* KO suggests that cell fate has not changed, but rather commitment to the midbrain DA NPC lineage may be impaired.

The significant decrease in intensity of DA markers in NPCs suggests that HPRT has a specific role in programming dopaminergic cell fate. If this is the case, we would

expect that markers of more differentiated DA cells should show significant defects as well, since expression of mature markers is dependent on full expression of NPC markers such as *Nurr1* (*NR4A2*) (Saucedo-Cardenas et al., 1998) and *FOXA1/2* (Ferri et al., 2007), which continue to be expressed in more mature DA neurons. We differentiated DA NPCs for 30 days and performed immunocytochemistry (ICC) against TH and the mature neuronal stain TUJ1 (Figure 2A). An automated analysis of signal intensity across 13,271 imaged cells found an average TH signal reduction of 50.6% ($p < 0.05$) (Figure 2B). Western blot showed clear decreases in TH (down 67% \pm 14%, $p = 0.0168$) (Figure 2C) and supported this finding quantitatively using an expanded set of markers (*FOXA1*, down 60% \pm 13% [$p = 0.00267$], *FOXA2*, down 73% \pm 9.6% [$p = 0.0051$], and *LMX1A*, down 45% \pm 15% [$p = 0.0432$]). While we do detect weak TH staining in many cells without HPRT, fewer cells are TH positive than would be expected from the NPC marker stage, where almost all cells are positive for DA markers (but with less intensity). These data suggest that the decreased intensity of DA NPC cell-fate markers might alter cell-fate programming as NPCs mature and differentiate.

The decreased expression of TH should be reflected in the amount of dopamine that *HPRT1* KO cells produce. To test this hypothesis, we performed high-performance liquid chromatography (HPLC) measurements of dopamine and breakdown products of dopamine at 25 and 80 days of differentiation from DA NPCs (Figures 2D–2G). We found significant decreases in dopamine and derivatives of dopamine in *HPRT1* KO neurons, which were exacerbated as cells aged, likely reflecting the increase in DA production that occurs as these cells mature between 25 and 80 days. Given the potential cell-fate change at later developmental stages, but clear expression of DA markers at NPC stages, we opted to perform further studies in the NPC stage, reasoning that later stage outcomes are derivatives of early cell-fate problems.

Loss of adenosine and guanosine derivatives in dopaminergic cells is more pronounced than in cortical cells

Loss of HPRT prevents salvage of purines, which could ultimately lead to a lack of purine derivatives, including ATP and GTP (Figure 3A). To assess and compare the direct effects of HPRT deficiency in isogenic stem, cortical, and midbrain cells, we performed HPLC after metabolite extraction (Figure 3). First, we observed that both KO CN NPCs and KO DA NPCs exhibit large increases (~ 4 -fold) in hypoxanthine, an expected consequence of HPRT deficiency observed in patients with LND across cell types (Fu et al., 2015). No such effect was seen in KO iPSCs, where HPRT is detectable; however, we cannot

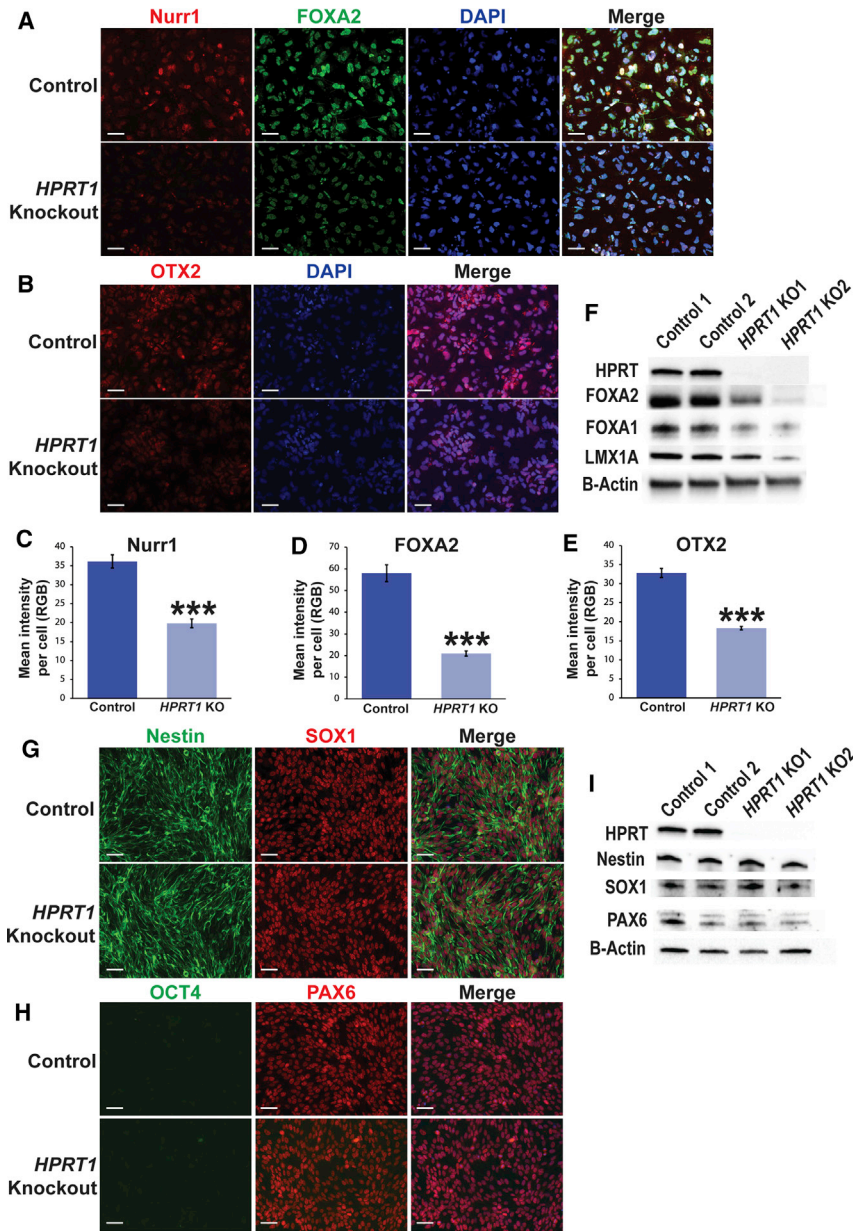


Figure 1. *HPRT1* knockout reduces the intensity of cell-fate markers in committed midbrain dopaminergic neural progenitor cells

n = 2 independent iPSC-derived clones from one control individual, and 2 different KO editing events from the same individual throughout this figure. Replicates are different clones and independent analyses from the same cell line.

(A) ICC for dopaminergic markers Nurr1 (NR4A2) and FOXA2 in *HPRT1* KO and control DA NPCs. Scale bar represents 50 μ m.

(B) ICC for dopaminergic marker OTX2 in *HPRT1* KO and control DA NPCs. Scale bar represents 50 μ m.

(C) Mean signal intensity per cell area from Nurr1 ICC images, as measured in QuPath. Data are derived from four separate cell lines (two control and two KO from a single individual). Eight images were used per cell line. Significance is based on Student's t test (**p < 0.01).

(D) Mean signal intensity per cell area from FOXA2 ICC images, as measured in QuPath. Data are derived from four separate cell lines (two control and two KO from a single individual). Eight images were used per cell line. Significance is based on Student's t test (**p < 0.01).

(E) Mean signal intensity per cell area from OTX2 ICC images, as measured in QuPath. Data are derived from four separate cell lines (two control and two KO from a single individual). Eight images were used per cell line. Significance is based on Student's t test (**p < 0.01).

(F) Western blots for dopaminergic markers in *HPRT1* KO and control DA NPCs.

(G) ICC for Nestin and SOX1 in *HPRT1* KO and control CN NPCs. Scale bar represents 50 μ m.

(H) ICC for OCT4 and PAX6 in *HPRT1* KO and control CN NPCs. Scale bar represents 50 μ m.

(I) Western blots for cortical markers in *HPRT1* KO and control CN NPCs.

rule out increased hypoxanthine excretion to the cell culture medium, as has been reported in stem cells (Sutcliffe et al., 2021). With respect to adenosine and guanosine derivatives, we observed decreased levels of almost all metabolites in HPRT-deficient NPCs, with consistently higher levels detected in DA cells than in CN, even independent of HPRT deficiency (Figures 3B and 3C). iPSCs had consistently lower levels of purine metabolites than DA or CN NPCs and showed no decrease in purine levels when *HPRT1* was deleted, consistent with hypoxanthine concentrations. These data provide evidence that DA pro-

genitors, morphologically indistinguishable from CN progenitors, have higher metabolic rates than forebrain cells, given higher baseline levels of adenine and guanine derivatives, even in healthy cells. This is surprising because midbrain DA cells are thought to have higher metabolic rates, due to pacemaker activity, and extensive connectivity (Mamelak, 2018; Pacelli et al., 2015), which are properties of terminally differentiated cells. This suggests that DA cells might be programmed very early on to have higher metabolic rates prior to cell maturation consisting of highly arborized morphology and pacemaker activity.

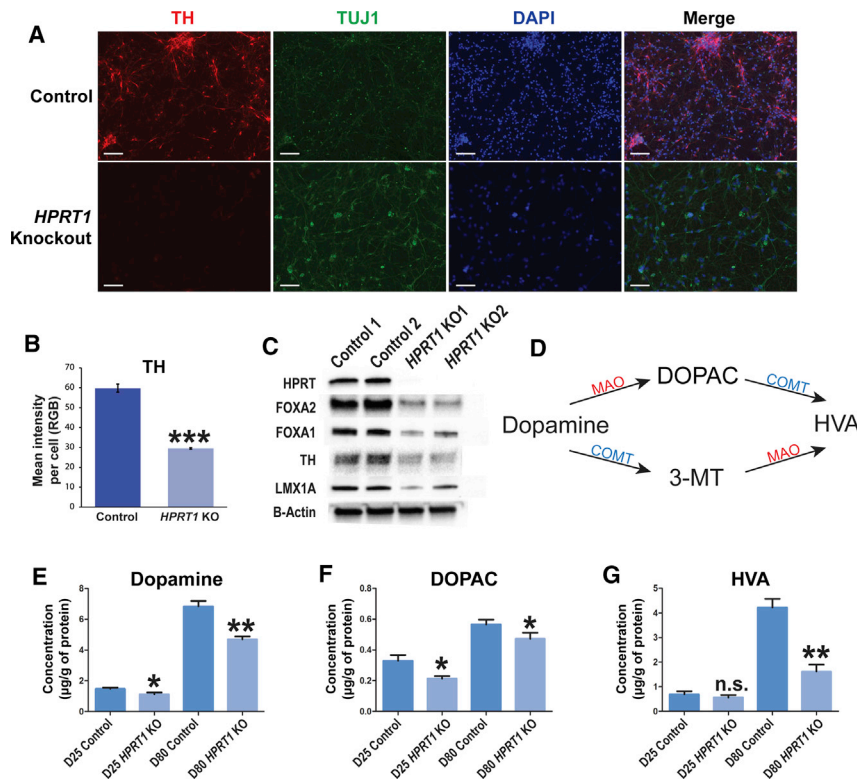


Figure 2. *HPRT1* knockout leads to loss of cell identity and dopaminergic metabolites in dopaminergic neurons

n = 2 independent iPSC-derived clones from one control individual, and 2 different KO editing events from the same individual throughout this figure. Replicates are different clones and independent analyses from the same cell line.

(A) ICC for the dopaminergic marker TH in *HPRT1* KO and control DA neurons. Scale bar represents 50 µm.

(B) Mean signal intensity per cell area from TH ICC images, as measured in QuPath. Data are derived from four separate cell lines (two control and two KO from a single individual). Eight images were used per cell line. Significance is based on Student's t test (***) $p < 0.001$.

(C) Western blots for dopaminergic markers in *HPRT1* KO and control DA neurons.

(D) Diagram of dopamine metabolism.

(E–G) HPLC measurements of dopamine, 3,4-dihydroxyphenylacetic acid (DOPAC), and homovanillic acid (HVA) in day 25 and day 80 *HPRT1* KO and control neurons. Significance is based on Student's t test comparing *HPRT1* KO to control

cells at matched time points (* $p < 0.05$, ** $p < 0.01$). n = 4 separate cell lines with four replicates used per cell line for 16 total data points.

Significant loss of glycolysis and oxidative phosphorylation potential due to *HPRT* deficiency

To assess the effects of *HPRT* deficiency on metabolism in DA and CN cells, oxidative phosphorylation (OXPHOS) and glycolytic potential (Figure 4A) were evaluated after drug challenge in real time. To this end, we simultaneously measured both oxygen consumption and extracellular acidification in genotypically matched DA and CN NPCs (Figures 4B and 4C). Consistent with our metabolite HPLC data, we found that control CN NPCs are less metabolically active than control DA NPCs, and that *HPRT1* defects in DA cells significantly impair both glycolysis and OXPHOS. In CN NPCs, we detected a significant decrease in glycolysis, but not OXPHOS (Figures 4B and 4C). This impairment may be due to the specific increased metabolic needs in DA NPCs, which cannot be met without purine salvage.

The abundance of mitochondria in a cell can fluctuate with energy state and have a significant impact on cellular metabolism (Liesa et al., 2009). We examined *TOMM20* expression, which is used as a marker of mitochondria, in DA NPCs and found no qualitative differences between *HPRT1* KO and isogenic controls (Figure S3C). This was supported by unchanged expression of *TFAM* RNA, a key

mitochondrial transcription factor, in *HPRT*-deficient compared with isogenic control DA NPCs (Figure S3D). We conclude that OXPHOS is specifically affected in DA NPCs lacking *HPRT* and that this is unlikely to be due to physiological changes in mitochondria.

More glucose shunted to the pentose phosphate pathway (PPP) and increased *de novo* purine synthesis in *HPRT*-deficient DA cells

The loss of glycolysis and OXPHOS potential might reflect increased utilization and flux of glucose to the PPP to create new purines at the expense of glycolysis and OXPHOS. We measured several metabolites known to be important in DA NPCs to determine if the PPP (Figure 4A) is more active in *HPRT*-deficient DA NPCs. We found increased levels of R5P and PRPP and AICAR, an intermediate product in *de novo* purine synthesis (Figure 4D). We also assessed AMP and IMP levels and included a measure of lactate as a readout for glycolytic flux. Lactate levels were decreased in *HPRT*-deficient cells, and levels of AMP and IMP (Figure 4D) were consistent with our previous results. This supports a hypothesis where glucose is shunted to a 5-carbon sugar to make purines, possibly at the expense of glycolysis and OXPHOS. Glucose can

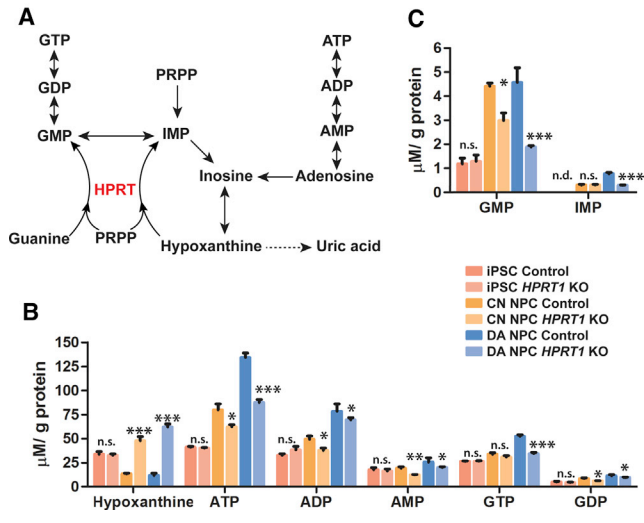


Figure 3. HPRT1 knockout depletes purine metabolites in midbrain and cortical neural progenitor cells
 n = 2 independent iPSC-derived clones from one control individual, and 2 different KO editing events from the same individual throughout this figure. Replicates are different clones and independent analyses from the same cell line.
 (A) Diagram of purine metabolism.
 (B and C) HPLC measurements for purine metabolites in iPSCs, cortical NPCs, and dopaminergic NPCs in HPRT1 KO and isogenic controls. Significance is based on Student's t test comparing HPRT1 KO to control cell within each cell type. Six to eight replicates were used for each cell line (*p < 0.05, **p < 0.01, ***p < 0.001; n.s., not significant; n.d., not detected).

also be utilized to create glycoproteins via the glycosylation pathway (Reily et al., 2019). We assessed glycoprotein synthesis to determine if glycosylation rate was affected by HPRT deficiency, but we detected no significant change in glycosylation state in HPRT-deficient DA and CN NPCs (Figures S4A and S4B).

To unequivocally demonstrate increased shunting of glucose to the PPP in HPRT-deficient DA NPCs, we exposed cells to a ¹³C-glucose medium for 4 h before extracting metabolites. This allows tracking of any metabolites that incorporate ¹³C. We found increased ¹³C in the R5P, PRPP, and AICAR metabolite pools in HPRT-deficient DA NPCs compared with control DA NPCs (Figure 4E). HPRT-deficient DA NPCs also had less ¹³C-containing lactate than isogenic control DA NPCs, a measure of glycolysis (Figure 4E). Finally, we found that levels of ¹³C in AMP and IMP were increased in HPRT-deficient DA NPCs compared with isogenic controls, suggesting a model whereby glucose is shunted to the PPP at the expense of energy metabolism and where the higher rate of *de novo* synthesis in HPRT-deficient DA NPCs is not sufficient to restore purine levels to baseline conditions (Figures 2D and 2E).

Inhibition of mTORC1 in HPRT-deficient dopaminergic cells but not cortical cells

We next sought to characterize the response of metabolic sensors to these metabolic imbalances. We investigated RHEB, a sensor of purine levels in cells (Hoxhaj et al., 2017) and required driver of mTORC1 (Figure 5A). HPRT deficiency strongly reduced RHEB levels in DA NPCs, but not in iPSCs or CN NPCs (Figure 5B), showing remarkable cell-type selectivity. If RHEB is indeed a purine sensor, this result suggests that only DA NPCs deficient in HPRT have purine loss drastic enough to trigger this sensor and impair mTORC1 as a result, possibly due to higher energy demands in DA NPCs. To test this, we selected two output markers of mTORC1 activity, ULK1 and RPS6, both of which are commonly used to monitor mTORC1 activity (Yanagiya et al., 2012). HPRT-deficient DA NPCs showed reduced levels of phosphorylation in ULK1 at residue 757 (Figure 5B), an exclusive target of mTORC1 (Chan et al., 2009). Because of the association between mTORC1, sonic hedgehog (SHH) signaling via GLI2, and dopaminergic cell development (Wu et al., 2017; Yan et al., 2016), we also examined if GLI2 levels were decreased in DA NPCs. Since less mTORC1 activation leads to less p757-ULK1, and phosphorylation of this site removes the brake on autophagy, we wanted to confirm that autophagy was increased with a real-time autophagy assay, involving starvation and autophagosome formation blockade by bafilomycin A in living cells (Figure 5C). In HPRT-deficient DA NPCs, we observed increased LC3-II (lower band) under autophagosome blockade, starvation only, and both starvation and autophagosome blockade together. This suggests that both baseline autophagy and starvation-induced autophagy are increased with HPRT deficiency, an effect that could be triggered by the depletion of RHEB and subsequent loss of mTORC1 activity.

Ribosomal protein S6 is downstream of mTORC1 and it can be activated by phosphorylation at position 240/244 (Meyuhas, 2015) (Figure S4C). Despite cell-line-specific variation, triplicate Western blot analysis detected a significant drop in 240/244 phosphorylation in DA NPCs, but not in CN NPCs (Figures S4D and S4D). These data support the idea that mTORC1 is less active when HPRT is deficient in DA NPCs. Ribosomal protein S6 is associated with protein synthesis of particular mRNAs (Meyuhas, 2015), so we attempted a real-time protein synthesis assay using the SUNSET assay (Schmidt et al., 2009). HPRT1 KO DA NPCs failed to show any significant difference in protein synthesis (Figure 5E), although this may be due to reported ambiguous p240/244-S6 effects on translation (Biever et al., 2015).

We were intrigued by the data suggesting increased autophagy via the decreases in p757-ULK1. Autophagy is reported to affect cilia, a signaling organelle for SHH required

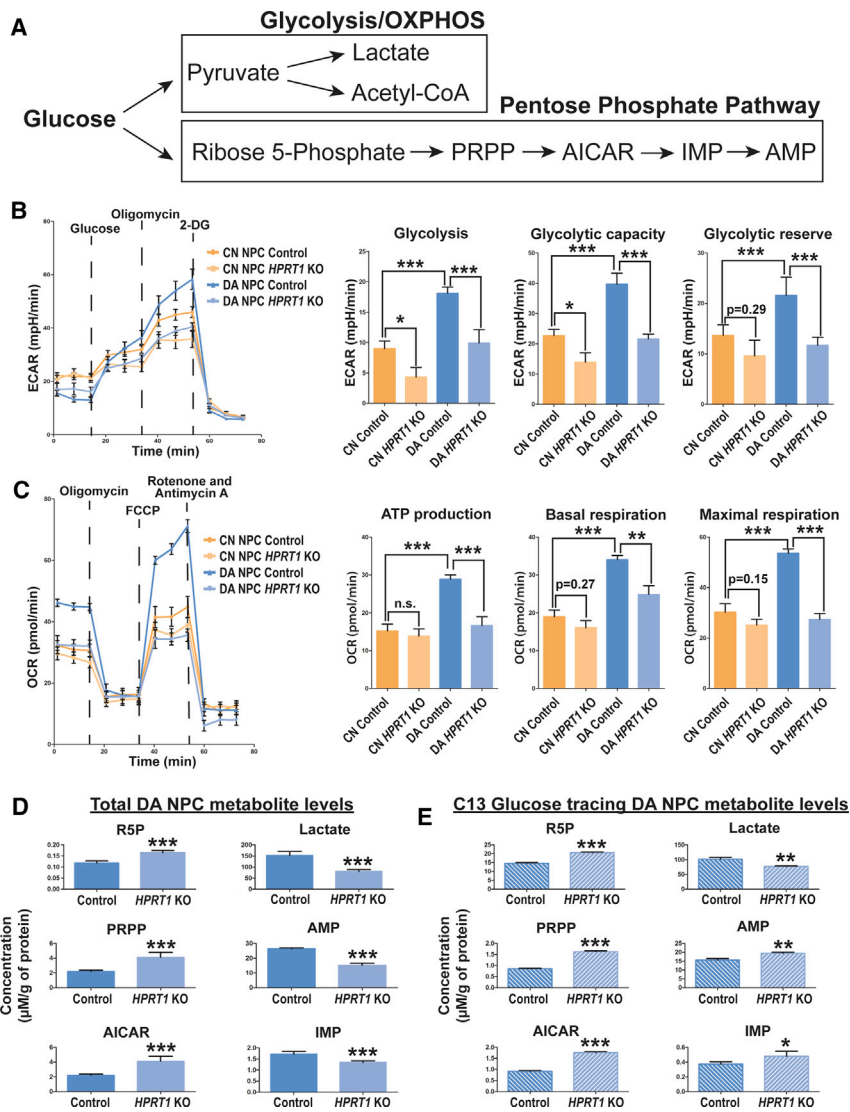


Figure 4. Differential effects of *HPRT1* knockout on glycolysis, oxidative phosphorylation, and glucose utilization in midbrain and cortical NPCs

n = 2 independent iPSC-derived clones from one control individual, and 2 different KO editing events from the same individual throughout this figure, except where indicated. Replicates are different clones and independent analyses from the same cell line.

(A) Diagram showing possible destinations of glucose of metabolites.

(B) Glycolysis measurements made via a Seahorse measurement of extracellular acidification. Graphs on the right summarize the data displayed on the left. Significance is based on a one-way ANOVA (*p < 0.05, ***p < 0.001). n = 4 separate cell lines with at least three or four replicates per line. 2-DG, 2-deoxyglucose.

(C) Oxidative phosphorylation measurements made via a Seahorse measurement of oxygen consumption. Bar graphs on the right summarize the data displayed on the left. Significance is based on a one-way ANOVA (**p < 0.01, ***p < 0.001). n = 4 separate cell lines with three or four replicates per line. FCCP, carbonyl cyanide 4-(trifluoromethoxy)phenylhydrazone.

(D) HPLC measurements of metabolites in the PPP and glycolytic pathways measured in *HPRT1* KO and isogenic control DA NPCs. n = 2 cell lines (one control and one KO) and three or four replicates per line. Significance is based on Student's t test (**p < 0.01, ***p < 0.001).

(E) C13 levels of metabolites in *HPRT1* KO and isogenic control DA NPCs 2 h after being

exposed to C13 glucose. n = 2 cell lines (one control and one KO) with three or four replicates per line. Significance is based on Student's t test (*p < 0.05, **p < 0.01, ***p < 0.001).

for DA cell development (Hynes et al., 1995). Autophagy is necessary for cilia growth, and ciliary signaling appears to affect autophagy (Pampliega and Cuervo, 2016). It is theoretically possible that autophagy affects DA cell development by influencing cilia length and frequency. To test this hypothesis, we measured cilia length and occurrence throughout the development of iPSCs into DA NPCs (Figure S5A) by visualizing cilia using combined IFT88 and acetylated tubulin, as well as ARL13B (Figure S5B). We found no evidence of significant difference in either cilia length or the proportion of ciliated cells at any developmental time point assessed (Figures S5C and S5D). These data suggest cilia dynamics are normal during differentiation from stem cells to DA NPCs and may suggest that

the DA-specific deficiencies caused by HPRT loss begin once cells are in a purified, committed, and higher energy DA progenitor state.

AMPK is a sensor of the AMP/ATP ratio and suppresses mTORC1 via phosphorylation of RAPTOR and TSC2 (Cork et al., 2018). As ATP levels drop and AMP levels rise, AMPK undergoes a conformational change, by the replacement of ATP by AMP in the active site of AMPK. This event leads to increased phosphorylation of residues Thr 172 and Thr 183 of AMPK, allowing the kinase to become active to restore ATP levels (Figure S6A). We have found that HPRT deficiency in DA NPCs leads to proportional decreases in ATP and AMP (Figure S6B, derived from data in Figure 3B), which might suggest that AMPK

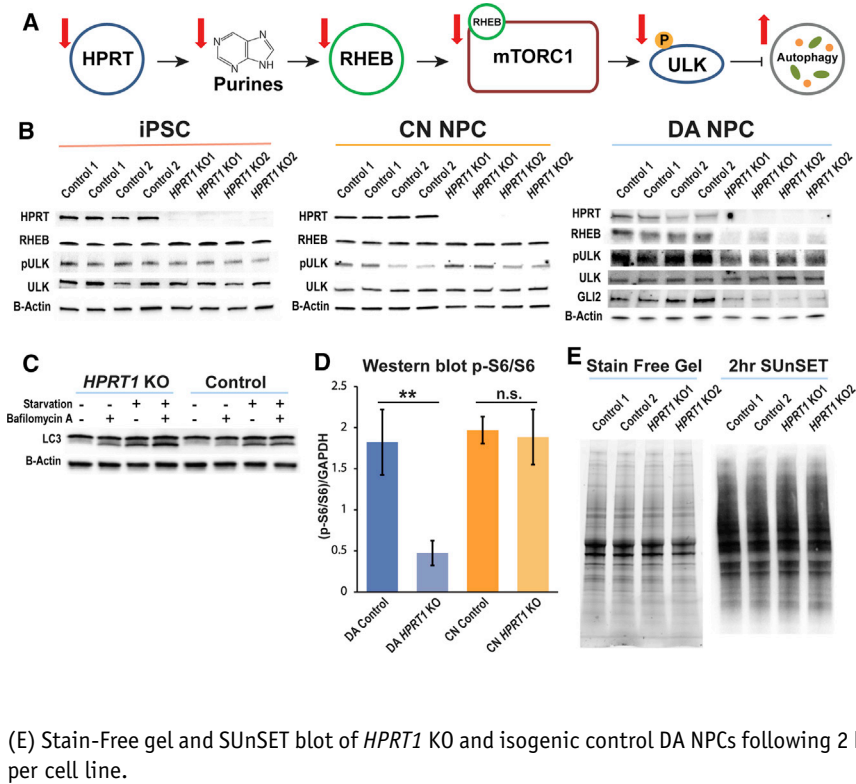


Figure 5. *HPRT1* knockout leads to decreased mTORC1 activity in midbrain NPCs, but not in cortical NPCs or iPSCs

$n = 2$ independent iPSC-derived clones from one control individual, and 2 different KO editing events from the same individual throughout this figure. Replicates are different clones and independent analyses from the same cell line.

(A) Diagram illustrating how a decrease in HPRT activity relates to mTORC1 activity and autophagy.

(B) Western blots showing markers of mTORC1 activity in *HPRT1* KO and isogenic control iPSCs, CN NPCs, and DA NPCs. Two replicates per cell line.

(C) Western blot of LC3-I and LC3-II levels in control and isogenic *HPRT1* KO DA NPCs when exposed to 8 h of serum starvation and/or 10 nM bafilomycin A. One replicate per cell line.

(D) Western blot quantification for the ratio of p240/244-S6 to total S6 normalized to GAPDH for blots shown in Figure S4D. Three replicates per cell line (** $p < 0.01$).

(E) Stain-Free gel and SUnSET blot of *HPRT1* KO and isogenic control DA NPCs following 2 h of exposure to 10 μ M puromycin. One replicate per cell line.

is not activated, even in the case of the severe loss of ATP in HPRT deficiency. That said, exogenously applied AICAR, which is high under our conditions, is a commonly used stimulator of AMPK (Sun et al., 2007) and is of interest because of its transformation to 5-amino-1- β -D-ribofuranosylimidazole-4-carboxamide monophosphate (ZMP), which has been associated with LND (Sidi and Mitchell, 1985). To assess this idea, we measured both p172/183 in AMPK and its target site in RAPTOR (Ser 722/792) (Gwinn et al., 2008) from HPRT KO DA NPCs and controls (Figures S6C–S6E). We found no difference in AMPK or RAPTOR phosphorylation states, meaning that AMPK does not affect energy deficits via mTORC1 or otherwise in DA NPCs deficient in HPRT.

Eight Lesch-Nyhan disease and variant cases recapitulate the effects of HPRT deficiency on cell-fate marker expression and OXPHOS

To externally validate the *HPRT1* KO data in people affected with disease and to demonstrate molecular effects on different genetic backgrounds, we made DA NPCs from three LND subjects, five LNV subjects, and four controls (Table S1) (Figure 6A). To minimize variability, the 12 fibroblast cell lines were reprogrammed to iPSCs simultaneously and then immediately differentiated to dopaminergic NPCs and neurons, when they were evaluated for metabolic effects and markers of dopaminergic fate.

A metabolic screen of PPP metabolites, identical in design to the KO studies, showed significant effects in all metabolites assessed in LND cells, with LNV cells showing an intermediate molecular phenotype between control and LND (Figure 6B). We found significant decreases in OXPHOS output measures in DA NPCs derived from HPRT-deficient subjects, with LNV subjects showing OXPHOS rates approximately intermediate to LND subjects and controls, accordant with the level of HPRT enzymatic activity but in a non-linear relationship (Figures 6C–6E). Finally, we found reduced protein levels of DA NPC markers and mTORC1 outputs in LND and LNV DA NPCs (Figure 6F). The expression of DA markers in LND-derived NPCs compared with controls showed deficits in FOXA1 (78% \pm 6% reduction compared with controls, $p \leq 0.0001$), FOXA2 (63% \pm 15%, $p = 0.0007$), LMX1A (75% \pm 19%, $p = 0.0178$), and GLI2 (59% \pm 10% $p \leq 0.0004$). Reduction in markers for LNV and LND samples were consistent with a one-phase decay exponential relationship, suggesting that most of the effect of HPRT deficiency on the expression of these proteins occurs as HPRT approaches complete loss (Figure 6G), providing *in vitro* support for why <1% activity might lead to such a severe clinical outcome compared with enzymatic activity greater than 2%; that is, the effect of HPRT loss on OXPHOS and DA markers is not linear. We differentiated all NPC lines from all three groups ($n = 12$) for 30 days and then

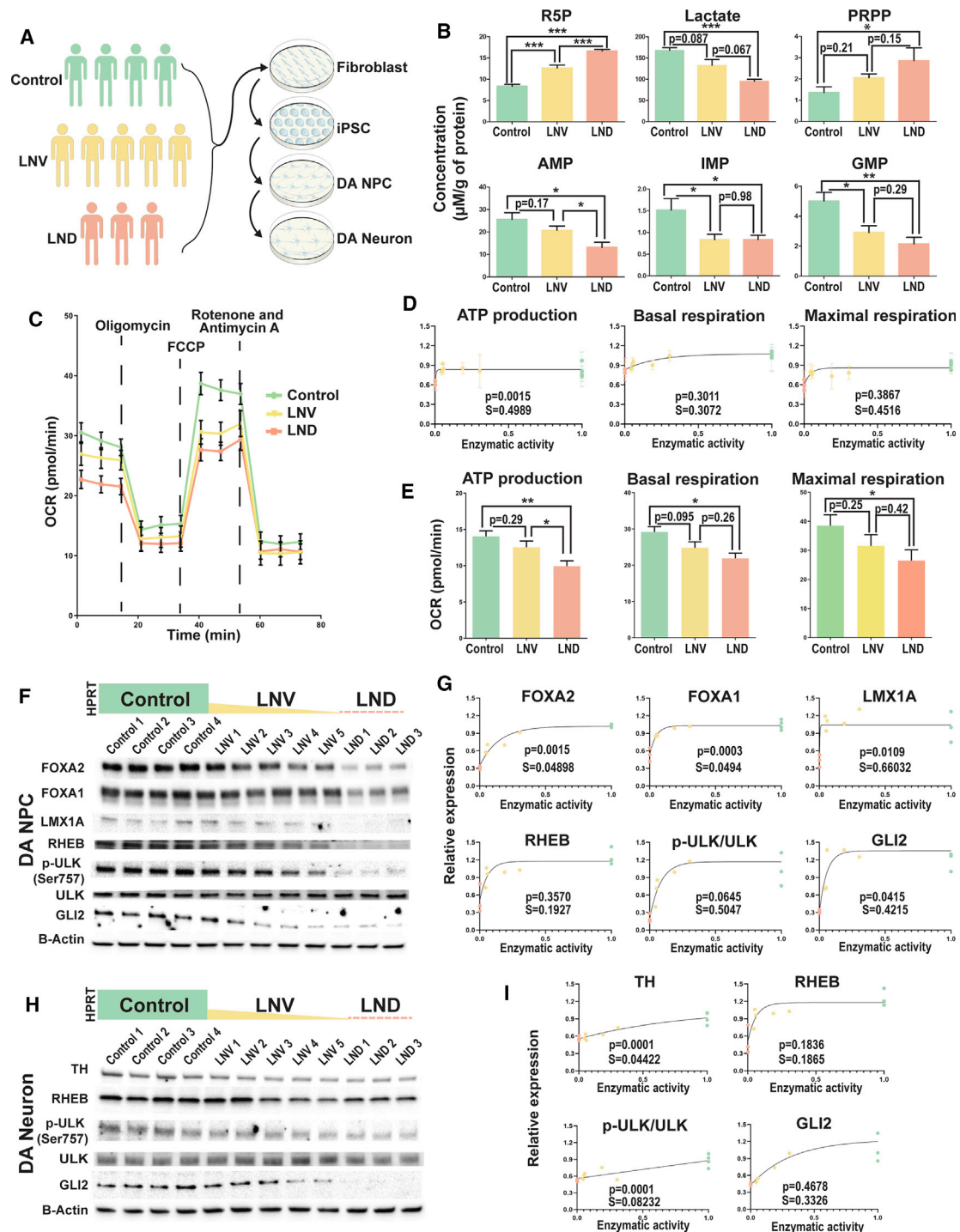


Figure 6. LNV and LND cases reveal significant relationships between enzyme activity, OXPHOS potential, and dopaminergic marker expression in NPCs and neurons

All data are derived from four controls, five LNV subjects, and three LND subjects throughout this figure (n = 12 cell lines from 12 different people).

(A) Diagram illustrating the process of generating dopaminergic cells from four control, five LNV, and three LND subjects.

(B) HPLC measurements of metabolites from the patient cohort. Significance is based on Student's t test comparing LND and LNV patient cohorts to controls (*p < 0.05, **p < 0.01, ***p < 0.001). Three or four replicates per cell line.

(legend continued on next page)



performed Western blot for mTORC1 and DA markers in neurons (Figure 6H) and plotted these against HPRT enzymatic activity (Figure 6I). We observed relationships similar to what we found in DA NPCs, that is, less HPRT activity corresponded with fewer DA markers in neurons and less mTORC1 activity, and this relationship is non-linear except for TH and ULK1. The presence of these deficits in post-mitotic cells suggests deficits persist throughout development once in place in NPCs.

DISCUSSION

Our data suggest that cell-type-specific experiments are essential to investigate HPRT dysfunction, since the intrinsic energy state may determine whether *de novo* synthesis can compensate for purine salvage loss. A specific threshold of energy impairment may need to be reached before a cell's developmental fate is compromised. DA cells have a higher background metabolic rate than CN cells and expose HPRT impairments as problems in energy metabolism, which can be obscured in cells without high-energy states. This was surprising because the high metabolic rates observed in midbrain DA cells uncovered in studies of Parkinson's disease have long been thought to be due to processes seen only in mature, post-mitotic cells (Mamelak, 2018; Pacelli et al., 2015). Our data show that DA cells are developmentally programmed for higher metabolic rates prior to any neurite branching and in the presumed absence of autonomous cell firing. It therefore seems probable that the programming of this metabolic activity may allow for the development of the energy-intensive processes seen in mature ventral midbrain DA cells, rather than vice versa.

Our investigation into glucose usage clarifies several long-standing questions for purine salvage deficiency studies. First, our data show that glucose is shunted to the PPP to increase *de novo* purine synthesis and that this is done at the expense of glycolysis and OXPHOS. We detected no changes in glycosylation levels, which suggests that that system likely remains intact. Our ^{13}C tracer experiments reveal that there are more purines being produced in HPRT-deficient DA cells, but that this level is not sufficient to compensate for the loss of purine salvage. While the cell may bring in more glucose, shunting glucose to *de novo* synthesis might remove product from the glucose budget and negatively affect glycolysis and OXPHOS. Loss of purine salvage results in significant deficits in midbrain DA progenitor glycolysis and OXPHOS, with cortical cells displaying only slight but significant deficits in glycolysis. This result may suggest that HPRT deficiency compromises the energy state of DA NPCs by reducing the ability of the cell to maintain an appropriately high level of OXPHOS.

DA progenitor cells likely sense the metabolic changes brought on by HPRT deficiency at least in part through the purine sensor RHEB, an obligate activator of mTORC1 (Emmanuel et al., 2017; Hoxhaj et al., 2017). RHEB is significantly depleted in HPRT-deficient cells, a result that has been shown in other experimental systems when purines are absent (Hoxhaj et al., 2017). This implies that mTORC1 cannot be fully activated, which may be important to drive DA cell differentiation. For example, in pancreatic cells mTORC1 is dispensable for α cell development but is essential for α cell maturation (Bozadjieva et al., 2017), which is driven by mTORC1 via FOXA2 and transcription of *ABCC8* (*Sur1*) and *KCNJ11* (*Kir6.2*), all of which are also markers of dopaminergic cells of the midbrain (Osborn and Hallett,

(C) Oxidative phosphorylation measurements made via Seahorse for control, LND, and LNV dopaminergic NPC lines. Oxygen consumption rate was measured as the drugs indicated on the dashed lines were applied in succession over 12.5 min intervals. Three or four replicates per cell line.

(D) Scatterplot showing the relationship between HPRT activity in DA NPCs and the level of ATP production, basal respiration, and maximal respiration. Parameters were calculated using the data displayed in (C) and color coded based on patient cohort. Curves were generated based on a line of best fit based on an equation for one-phase decay. The p values represent relative likelihood of a one-phase exponential decay versus a linear relationship, calculated using the Akaike information criterion.

(E) Bar graphs summarizing key parameters from the OXPHOS data displayed in (D) by patient cohort. Significance is based on Student's t test comparing LND and LNV patient cohorts to controls (* $p < 0.05$, ** $p < 0.01$).

(F) Western blot of control, LNV, and LND patient dopaminergic NPCs probed for dopaminergic and mTORC1 activity markers. All cell lines were lysed 24 ± 1 h after last medium exchange.

(G) Non-linear regression of protein expression data shown in (E). Curves were generated based on a line of best fit based on an equation for one-phase decay. The p values represent relative likelihood of a one-phase exponential decay versus a linear relationship, calculated using the Akaike information criterion.

(H) Western blot of control, LNV, and LND patient dopaminergic D15 neurons probed for dopaminergic and mTORC1 activity markers.

(I) Non-linear regression of protein expression data shown in (H). Curves were generated based on a line of best fit based on an equation for one-phase decay, for GLI2 and RHEB, and a linear line of best fit for TH and pULK/total ULK. The p values represent relative likelihood of a one-phase exponential decay versus a linear relationship, calculated using the Akaike information criterion.



2017). These data suggest that mTORC1 activation is important for cell differentiation and activation of FOXA2, and also that mTORC1 has a role in midbrain dopaminergic cells, although we cannot rule out mTORC1 being a passenger of some other as of yet unidentified driver effect.

The loss of DA markers correlates with the degree of loss of enzymatic activity of HPRT, suggesting a strong association between purine salvage and midbrain cell development. While no single marker is definitive of midbrain DA cells, analysis of all suggests that purine salvage must be intact for proper differentiation of this cell type. It is tempting to speculate that the deficits in OXPHOS and ATP production we observed early on in DA programming lead to the loss of marker potential, but we warn against this simplistic interpretation. We cannot rule out that the DA markers drive the metabolic deficits, or that the two processes are intertwined. FOXA1/2 (aka HNF3a/b), for example, are well known glucose-response genes in the pancreas (Hedddad Masson et al., 2014) and are essential for DA development according to mouse KO studies (Gao et al., 2010). Indeed, mouse FOXA1/2 KO shows reduced TH staining with variable loss of DA cells (Pristerà et al., 2015), a situation very similar to what is observed in post-mortem LND brains (Göttle et al., 2014).

Conclusion

The heightened energy state of DA progenitor cells may be restricted by some feature or constellation of proteins observed in stem cells, hindering differentiation of DA NPCs due to the inability to shift from *de novo* synthesis to purine salvage. Preserving or reverting to a “stem-like” state might ensure enough purines for a cell by relying on *de novo* synthesis, but these stem cell proteins might also inhibit differentiation, which could explain why DA NPCs still meet criteria for DA NPCs, but with less intense staining. Decreased cell death with HPRT loss may also be a feature of cells more reliant on *de novo* synthesis rather than salvage. Precisely what DA NPCs deficient in HPRT become after terminal differentiation is not currently known, although we favor a surrounding cell type of the substantia nigra such as red nucleus cell subtypes.

EXPERIMENTAL PROCEDURES

Tables S1–S3 in the [supplemental information](#) outline the cell lines and antibodies used in this study. This work was approved by the research ethics board by the Douglas Hospital Research Institute.

CRISPR-Cas9 generation of *HPRT1* knockout

A double-nickase CRISPR-Cas9 gene editing system with gRNA (DNA2.0) targeting a 13 bp exonic sequence of *HPRT1* (AGTCCTA CAGAAATAAATC) was generated with a Paprika RFP reporter

(DNA 2.0). Five micrograms of this construct was added per transfection reaction, and transfection was carried out using the parameters described for iPSC induction. Following transfection, the cells were plated on Matrigel-coated plates in 10% FBS DMEM for 24 h. The cells were then detached and sorted via fluorescence-activated cell sorting for RFP⁺ cells. RFP⁺ cells were then replated on Matrigel-coated plates in 10% FBS DMEM supplemented with 2 µg/mL puromycin. Following 48 h of selection, the cells were dissociated using 0.05% EDTA-trypsin and plated in Matrigel-coated six-well tissue culture plates (Corning) in TesR-E7 medium at a density of ~1,000 cells per well. Colony formation, picking, and purification proceeded as described for iPSC induction.

Reprogramming to induced pluripotent stem cells

Fibroblasts were cultured in DMEM (Invitrogen) supplemented with 10% BSA (Invitrogen). The cells were then reprogrammed using episomal reprogramming vectors containing Oct4, Sox2, Myc3/4, Klf4, ShRNA P53 (ALSTEM), and a puromycin-resistance gene using the Neon transfection system (Invitrogen). Following transfection, the cells were plated on tissue culture plates coated with Matrigel (Corning) in TesR-E7 medium (STEMCELL Technologies) supplemented with 2 µg/mL puromycin (Sigma). After 48 h of puromycin selection, fresh TesR-E7 medium was provided, until distinct and robust iPSC colonies formed, at which point mTESR1 medium (STEMCELL Technologies) was used to maintain and proliferate the colonies.

Induction of iPSCs to neural progenitor cells

iPSC colonies were dissociated and resuspended in DMEM/F12 medium supplemented with N2 (Invitrogen), B27 (Invitrogen) and BSA (1 mg/mL), Y27632 (10 µM; AdooQ Bioscience), SB431542 (10 mM; Selleckchem), and Noggin (200 ng/mL; GenScript) onto non-adherent plates to form organoids. After 1 week of maintenance as organoids, the cells were dissociated and plated on Matrigel-coated plates in DMEM/F12 supplemented with B27, bFGF (20 ng/mL), EGF (20 ng/mL), and laminin (1 µg/mL) for a further 7 days of differentiation, with the medium exchanged every 3 days. Cells were assessed for NPC morphology and stained for markers of forebrain NPCs (PAX6, SOX2, TUJ1) and OCT4.

Differentiation of NPCs to post-mitotic neurons

Differentiation was initiated when NPCs reached 70% confluency. Medium was exchanged for DMEM/F12 supplemented with B27, GDNF (2 µM, GenScript), BDNF (1 µM, GenScript), and laminin (1 µg/mL). Cells were maintained in this medium, with half the medium exchanged every 2 days until the cells achieved the desired developmental time point.

Quantification of cell identities (immunocytochemistry)

ICC quantification of Nurr1 (NR4A2), FOXA2, OTX2, and TH was performed using QuPath, with data collected from 32 images for each analysis. For each image, cell areas were defined using cell detection in the DAPI channel. The mean signal intensity (value between 0 and 255) within the area defined by cell detection was recorded for each image. An overall average across the 16 images from each genotype was determined. Analyses for Nurr1 and



FOX2 in DA NPC involved mean signal intensity measurements from 3,719 detected cells. The analysis for OTX2 in DA NPC involved mean signal intensity measurements from 4,634 detected cells. The analysis for TH in neurons involved mean signal intensity measurements from 13,271 detected cells.

SUPPLEMENTAL INFORMATION

Supplemental information can be found online at <https://doi.org/10.1016/j.stemcr.2021.06.003>.

AUTHOR CONTRIBUTIONS

S.B., V.M., and C.E. wrote the manuscript and were involved in all aspects of the design and execution of the study. H.P., M.J., N.H., L.A., L.C., L.A.O., X.Z., Y.Z., H.W., and I.K. performed experiments. D.S., N.M., and H.A.J. contributed reagents and advised on study design; T.A.R., L.M., and A.G. performed HPLC. J.P., I.G., and N.S. performed and interpreted protein assays related to mTORC1; P.S.S. and A.A.S. performed statistical analyses. M.L.T. coordinated and supervised the Seahorse experiments.

ACKNOWLEDGMENTS

Robert Flick at the University of Toronto's BioZone facility performed all metabolic analyses. Daina Avizonis and Gaelle Bridon established pilot metabolic data at McGill facilities. Jeff Gross and LifeLabs Genetics performed genomic integrity analysis. All images were taken at the Molecular and Cellular Microscopy Platform at the Douglas Hospital Research Center. C.E. is funded by a Canada Research Chair and this work was supported in part by the CIHR. This work was also supported in part by NIH R56 NS102980 and R01 NS109242.

Received: July 30, 2020

Revised: June 2, 2021

Accepted: June 3, 2021

Published: July 1, 2021

REFERENCES

Bell, S., Kolobova, I., Crapper, L., and Ernst, C. (2016). Lesch-Nyhan syndrome: models, theories, and therapies. *Mol. Syndromol.* *7*, 302–311. <https://doi.org/10.1159/000449296>.

Bell, S., Hettige, N.C., Silveira, H., Peng, H., Wu, H., Jefri, M., Antonyan, L., Zhang, Y., Zhang, X., and Ernst, C. (2019). Differentiation of human induced pluripotent stem cells (iPSCs) into an effective model of forebrain neural progenitor cells and mature neurons. *Bio Protoc.* *9*. <https://doi.org/10.21769/bioprotoc.3188>.

Biever, A., Valjent, E., and Puighermanal, E. (2015). Ribosomal protein S6 phosphorylation in the nervous system: from regulation to function. *Front. Mol. Neurosci.* *8*, 75. <https://doi.org/10.3389/fnmol.2015.00075>.

Bitler, C.M., and Howard, B.D. (1986). Dopamine metabolism in hypoxanthine-guanine phosphoribosyltransferase-deficient variants of PC12 cells. *J. Neurochem.* *47*, 107–112. <https://doi.org/10.1111/j.1471-4159.1986.tb02837.x>.

Bozadjieva, N., Blandino-Rosano, M., Chase, J., Dai, X.Q., Cummings, K., Gimeno, J., Dean, D., Powers, A.C., Gittes, G.K., Rüegg, M.A., et al. (2017). Loss of mTORC1 signaling alters pancreatic α cell mass and impairs glucagon secretion. *J. Clin. Invest.* *127*, 4379–4393. <https://doi.org/10.1172/JCI90004>.

Chan, E.Y., Longatti, A., McKnight, N.C., and Tooze, S.A. (2009). 'Kinase-Inactivated ULK proteins inhibit autophagy via their conserved C-terminal domains using an atg13-independent mechanism. *Mol. Cell Biol.* *29*, 157–171. <https://doi.org/10.1128/mcb.01082-08>.

Cork, G.K., Thompson, J., and Slawson, C. (2018). Real talk: the inter-play between the mTOR, AMPK, and hexosamine biosynthetic pathways in cell signaling. *Front. Endocrinol.* *9*, 522. <https://doi.org/10.3389/fendo.2018.00522>.

Costa, M.R.C., Edelstein, S.B., Castiglione, C.M., Chao, H., and Breakefield, X.O. (1980). Properties of monoamine oxidase in control and Lesch-Nyhan fibroblasts. *Biochem. Genet.* *18*, 577–590. <https://doi.org/10.1007/BF00484403>.

Cox, R.P., Krauss, M.R., Balis, M.E., and Dancis, J. (1970). 'Evidence for transfer of enzyme product as the basis of metabolic cooperation between tissue culture fibroblasts of Lesch-Nyhan disease and normal cells. *Proc. Natl. Acad. Sci. U S A* *67*, 1573–1579. <https://doi.org/10.1073/pnas.67.3.1573>.

Edelstein, S.B., Castiglione, C.M., and Breakfield, X.O. (1978). Monoamine oxidase activity in normal and lesch-nyhan fibroblasts. *J. Neurochem.* *31*, 1247–1254. <https://doi.org/10.1111/j.1471-4159.1978.tb06249.x>.

Egami, K., Yitta, S., Kasim, S., Lewers, J.C., Roberts, R.C., Lehar, M., and Jinnah, H.A. (2007). Basal ganglia dopamine loss due to defect in purine recycling. *Neurobiol. Dis.* *26*, 396–407. <https://doi.org/10.1016/j.nbd.2007.01.010>.

Emmanuel, N., Ragunathan, S., Shan, Q., Wang, F., Giannakou, A., Huser, N., Jin, G., Myers, J., Abraham, R.T., and Unsal-Kacmaz, K. (2017). Purine nucleotide availability regulates mTORC1 activity through the rheb GTPase. *Cell Rep.* *19*, 2665–2680. <https://doi.org/10.1016/j.celrep.2017.05.043>.

Ernst, M., Zemetkin, A.J., Matochik, J.A., Pascualvaca, D., Jons, P.H., Hardy, K., Hankerson, J.G., Doudet, D.J., and Cohen, R.M. (1996). 'Presynaptic dopaminergic deficits in lesch-nyhan disease'. *N. Engl. J. Med.* *334*, 1568–1572. <https://doi.org/10.1056/NEJM199606133342403>.

Ferri, A.L., Lin, W., Mavromatakis, Y.E., Wang, J.C., Sasaki, H., Whitsett, J.A., and Ang, S.L. (2007). Foxa1 and Foxa2 regulate multiple phases of midbrain dopaminergic neuron development in a dosage-dependent manner. *Development* *134*, 2761–2769. <https://doi.org/10.1242/dev.000141>.

Fu, R., Sutcliffe, D., Zhao, H., Huang, X., Schretlen, D.J., Benkovic, S., and Jinnah, H.A. (2015). Clinical severity in lesch-Nyhan disease: the role of residual enzyme and compensatory pathways. *Mol. Genet. Metab.* *114*, 55–61. <https://doi.org/10.1016/j.ymgme.2014.11.001>.

Gao, L., Zhou, W., Symmes, B., and Freed, C.R. (2016). Re-cloning the N27 dopamine cell line to improve a cell culture model of Parkinson's disease. *PLoS One* *11*, e0160847. <https://doi.org/10.1371/journal.pone.0160847>.



- Gao, N., Le Lay, J., Qin, W., Doliba, N., Schug, J., Fox, A.J., Smirnova, O., Matschinsky, F.M., and Kaestner, K.H. (2010). Foxa1 and Foxa2 maintain the metabolic and secretory features of the mature beta-cell. *Mol. Endocrinol.* *24*, 1594–1604. <https://doi.org/10.1210/me.2009-0513>.
- Garcia, D., and Shaw, R.J. (2017). AMPK: mechanisms of cellular energy sensing and restoration of metabolic balance. *Mol. Cell* *66*, 789–800. <https://doi.org/10.1016/j.molcel.2017.05.032>.
- Garza-Lombó, C., and Gonsebatt, M.E. (2016). Mammalian target of rapamycin: its role in early neural development and in adult and aged brain function. *Front. Cell. Neurosci.* *10*, 157. <https://doi.org/10.3389/fncel.2016.00157>.
- Göttle, M., Prudente, C.N., Fu, R., Sutcliffe, D., Pang, H., Cooper, D., Veledar, E., Glass, J.D., Gearing, M., Visser, J.E., and Jinnah, H.A. (2014). Loss of dopamine phenotype among midbrain neurons in Lesch-Nyhan disease. *Ann. Neurol.* *76*, 95–107. <https://doi.org/10.1002/ana.24191>.
- Gwinn, D.M., Shackelford, D.B., Egan, D.F., Mihaylova, M.M., Mery, A., Vasquez, D.S., Turk, B.E., and Shaw, R.J. (2008). AMPK phosphorylation of raptor mediates a metabolic checkpoint. *Mol. Cell* *30*, 214–226. <https://doi.org/10.1016/j.molcel.2008.03.003>.
- Heddad Masson, M., Poisson, C., Guérardel, A., Mamin, A., Philippe, J., and Gosmain, Y. (2014). Foxa1 and Foxa2 regulate α -cell differentiation, glucagon biosynthesis, and secretion. *Endocrinology* *155*, 3781–3792. <https://doi.org/10.1210/en.2013-1843>.
- Hoxhaj, G., Hughes-Hallett, J., Timson, R.C., Ilagan, E., Yuan, M., Asara, J.M., Ben-Sahra, I., and Manning, B.D. (2017). The mTORC1 signaling network senses changes in cellular purine nucleotide levels. *Cell Rep.* *21*, 1331–1346. <https://doi.org/10.1016/j.celrep.2017.10.029>.
- Hynes, M., Porter, J.A., Chiang, C., Chang, D., Tessier-Lavigne, M., Beachy, P.A., and Rosenthal, A. (1995). Induction of midbrain dopaminergic neurons by Sonic hedgehog. *Neuron* *15*, 35–44. [https://doi.org/10.1016/0896-6273\(95\)90062-4](https://doi.org/10.1016/0896-6273(95)90062-4).
- Jefri, M., Bell, S., Peng, H., Hettige, N., Maussion, G., Soubannier, V., Wu, H., Silveira, H., Theroux, J.F., Moquin, L., et al. (2020). ‘Stimulation of L-type calcium channels increases tyrosine hydroxylase and dopamine in ventral midbrain cells induced from somatic cells’. *Stem Cells Transl. Med.* *9*, 18–0180. <https://doi.org/10.1002/sctm.18-0180>.
- Jinnah, H.A., Visser, J.E., Harris, J.C., Verdu, A., Larovere, L., Ceballos-Picot, I., Gonzalez-Alegre, P., Neychev, V., Torres, R.J., Dulac, O., et al. (2006). ‘Delineation of the motor disorder of Lesch–Nyhan disease’. *Brain* *129*, 1201–1217. <https://doi.org/10.1093/brain/awl056>.
- Jinnah, H.A. (2009). Lesch-Nyhan disease: from mechanism to model and back again. *Dis. Models Mech.*, 116–121. <https://doi.org/10.1242/dmm.002543>.
- Jinnah, H.A., Ceballos-Picot, I., Torres, R.J., Visser, J.E., Schretlen, D.J., Verdu, A., Laróvere, L.E., Chen, C.J., Cossu, A., Wu, C.H., et al. (2010). Attenuated variants of Lesch-Nyhan disease. *Brain* *133*, 671–689. <https://doi.org/10.1093/brain/awq013>.
- Ka, M., Condorelli, G., Woodgett, J.R., and Kim, W.Y. (2014). mTOR regulates brain morphogenesis by mediating GSK3 signaling. *Development* *141*, 4076–4086. <https://doi.org/10.1242/dev.108282>.
- La, H.M., Chan, A.L., Legrand, J.M.D., Rossello, F.J., Gangemi, C.G., Papa, A., Cheng, Q., Morand, E.F., and Hobbs, R.M. (2018). GILZ-dependent modulation of mTORC1 regulates spermatogonial maintenance. *Development* *145*. <https://doi.org/10.1242/dev.165324>.
- Lesch, M., and Nyhan, W.L. (1964). A familial disorder of uric acid metabolism and central nervous system function. *Am. J. Med.* *36*, 561–570. [https://doi.org/10.1016/0002-9343\(64\)90104-4](https://doi.org/10.1016/0002-9343(64)90104-4).
- Lewers, J.C., Ceballos-Picot, I., Shirley, T.L., Mockel, L., Egami, K., and Jinnah, H.A. (2008). Consequences of impaired purine recycling in dopaminergic neurons. *Neuroscience* *152*, 761–772. <https://doi.org/10.1016/j.neuroscience.2007.10.065>.
- Liesa, M., Palacín, M., and Zorzano, A. (2009). Mitochondrial dynamics in mammalian health and disease. *Physiol. Rev.* *89*, 799–845. <https://doi.org/10.1152/physrev.00030.2008>.
- Mamelak, M. (2018). Parkinson’s disease, the dopaminergic neuron and gamma-hydroxybutyrate. *Neurol. Ther.* *7*, 5–11. <https://doi.org/10.1007/s40120-018-0091-2>.
- Meyuhas, O. (2015). Ribosomal protein S6 phosphorylation: four decades of research. *Int. Rev. Cell Mol. Biol.* *320*, 41–73. <https://doi.org/10.1016/bs.ircmb.2015.07.006>.
- Moffatt, B.A., and Ashihara, H. (2002). Purine and pyrimidine nucleotide synthesis and metabolism. *Arabidopsis Book 1*, e0018. <https://doi.org/10.1199/tab.0018>.
- Murakami, M., Ichisaka, T., Maeda, M., Oshiro, N., Hara, K., Edenhofer, F., Kiyama, H., Yonezawa, K., and Yamanaka, S. (2004). mTOR is essential for growth and proliferation in early mouse embryos and embryonic stem cells. *Mol. Cell Biol.* *24*, 6710–6718. <https://doi.org/10.1128/MCB.24.15.6710-6718.2004>.
- Osborn, T., and Hallett, P.J. (2017). Seq-ing markers of midbrain dopamine neurons. *Cell Stem Cell* *20*, 11–12. <https://doi.org/10.1016/j.stem.2016.12.014>.
- Pacelli, C., Giguère, N., Bourque, M.J., Lévesque, M., Slack, R.S., and Trudeau, L.É. (2015). Elevated mitochondrial bioenergetics and axonal arborization size are key contributors to the vulnerability of dopamine neurons. *Curr. Biol.* *25*, 2349–2360. <https://doi.org/10.1016/j.cub.2015.07.050>.
- Pampliega, O., and Cuervo, A.M. (2016). Autophagy and primary cilia: dual interplay. *Curr. Opin. Cell Biol.* *39*, 1–7. <https://doi.org/10.1016/j.ceb.2016.01.008>.
- Paul, G., Christophersen, N.S., Raymon, H., Kiaer, C., Smith, R., and Brundin, P. (2007). Tyrosine hydroxylase expression is unstable in a human immortalized mesencephalic cell line—Studies in vitro and after intracerebral grafting in vivo. *Mol. Cell. Neurosci.* *34*, 390–399. <https://doi.org/10.1016/j.mcn.2006.11.010>.
- Pedley, A.M., and Benkovic, S.J. (2017). A new view into the regulation of purine metabolism: the purinosome. *Trends Biochem. Sci.* *42*, 141–154. <https://doi.org/10.1016/j.tibs.2016.09.009>.
- Pristerà, A., Lin, W., Kaufmann, A.K., Brimblecombe, K.R., Threlfell, S., Dodson, P.D., Magill, P.J., Fernandes, C., Cragg, S.J., and Ang, S.L. (2015). Transcription factors FOXA1 and FOXA2 maintain dopaminergic neuronal properties and control feeding



- behavior in adult mice. *Proc. Natl. Acad. Sci. U S A* *112*, E4929–E4938. <https://doi.org/10.1073/pnas.1503911112>.
- Reily, C., Stewart, T.J., Renfrow, M.B., and Novak, J. (2019). Glycosylation in health and disease. *Nat. Rev. Nephrol.* *15*, 346–366. <https://doi.org/10.1038/s41581-019-0129-4>.
- Saucedo-Cardenas, O., Quintana-Hau, J.D., Le, W.D., Smidt, M.P., Cox, J.J., De Mayo, F., Burbach, J.P., and Conneely, O.M. (1998). Nurr1 is essential for the induction of the dopaminergic phenotype and the survival of ventral mesencephalic late dopaminergic precursor neurons. *Proc. Natl. Acad. Sci. U S A* *95*, 4013–4018. <https://doi.org/10.1073/pnas.95.7.4013>.
- Saxton, R.A., and Sabatini, D.M. (2017). mTOR signaling in growth, metabolism, and disease. *Cell* *168*, 960–976. <https://doi.org/10.1016/j.cell.2017.02.004>.
- Schmidt, E.K., Clavarino, G., Ceppi, M., and Pierre, P. (2009). SUNSET, a nonradioactive method to monitor protein synthesis. *Nat. Methods* *6*, 275–277. <https://doi.org/10.1038/nmeth.1314>.
- Sidi, Y., and Mitchell, B.S. (1985). Z-nucleotide accumulation in erythrocytes from Lesch-Nyhan patients. *J. Clin. Invest.* *76*, 2416–2419. <https://doi.org/10.1172/JCI112255>.
- Sun, Y., Connors, K.E., and Yang, D.Q. (2007). AICAR induces phosphorylation of AMPK in an ATM-dependent, LKB1-independent manner. *Mol. Cell. Biochem* *306*, 239–245. <https://doi.org/10.1007/s11010-007-9575-6>.
- Sutcliffe, D.J., Dinasarapu, A.R., Visser, J.E., Hoed, J.D., Seifar, F., Joshi, P., Ceballos-Picot, I., Sardar, T., Hess, E.J., Sun, Y.V., et al. (2021). Induced pluripotent stem cells from subjects with Lesch-Nyhan disease. *Sci. Rep.* *11*, 8523. <https://doi.org/10.1038/s41598-021-87955-9>.
- Takahashi, K., Tanabe, K., Ohnuki, M., Narita, M., Ichisaka, T., Tomoda, K., and Yamanaka, S. (2007). Induction of pluripotent stem cells from adult human fibroblasts by defined factors. *Cell* *131*, 861–872. <https://doi.org/10.1016/j.cell.2007.11.019>.
- Wang, H.X., Shin, J., Wang, S., Gorentla, B., Lin, X., Gao, J., Qiu, Y.R., and Zhong, X.P. (2016). mTORC1 in thymic epithelial cells is critical for thymopoiesis, T-cell generation, and temporal control of $\gamma\delta$ T17 development and $\text{tcr}\gamma/\delta$ recombination. *PLoS Biol.* *14*, e1002370. <https://doi.org/10.1371/journal.pbio.1002370>.
- Watts, R.W., Spellacy, E., Gibbs, D.A., Allsop, J., McKeran, R.O., and Slavin, G.E. (1982). Clinical, post-mortem, biochemical and therapeutic observations on the lesch-nyhan syndrome with particular reference to the neurological manifestations. *Q. J. Med.* *51*, 43–78. <https://doi.org/10.1093/oxfordjournals.qjmed.a067707>.
- Wu, C.C., Hou, S., Orr, B.A., Kuo, B.R., Youn, Y.H., Ong, T., Roth, F., Eberhart, C.G., Robinson, G.W., Solecki, D.J., et al. (2017). mTORC1-Mediated inhibition of 4EBP1 is essential for hedgehog signaling-driven translation and medulloblastoma. *Dev. Cell* *43*, 673–688.e5. <https://doi.org/10.1016/j.devcel.2017.10.011>.
- Yan, B., Zhang, Z., Jin, D., Cai, C., Jia, C., Liu, W., Wang, T., Li, S., Zhang, H., Huang, B., et al. (2016). mTORC1 regulates PTHrP to coordinate chondrocyte growth, proliferation and differentiation. *Nat. Commun.* *7*, 11151. <https://doi.org/10.1038/ncomms11151>.
- Yanagija, A., Suyama, E., Adachi, H., Svitkin, Y.V., Aza-Blanc, P., Imataka, H., Mikami, S., Martineau, Y., Ronai, Z.A., and Sonenberg, N. (2012). Translational homeostasis via the mRNA cap-binding protein, eIF4E. *Mol. Cell* *46*, 847–858. <https://doi.org/10.1016/j.molcel.2012.04.004>.
- Yeh, J., Zheng, S., and Howard, B.D. (1998). 'Impaired differentiation of HPRT-deficient dopaminergic neurons: a possible mechanism underlying neuronal dysfunction in Lesch-Nyhan syndrome'. *J. Neurosci. Res.* *53*, 78–85. [https://doi.org/10.1002/\(SICI\)1097-4547\(19980701\)53:1<78::AID-JNR8>3.0.CO;2-G](https://doi.org/10.1002/(SICI)1097-4547(19980701)53:1<78::AID-JNR8>3.0.CO;2-G).